Determination of dynamic variations in the optical properties of graphene oxide in response to gas exposure based on thin-film interference

SHAWANA TABASSUM,* LIANG DONG, AND RATNESH KUMAR

Department of Electrical and Computer Engineering, Iowa State University, Ames, IA 50011, USA
*tabassum@iastate.edu

Abstract: We present an effective yet simple approach to study the dynamic variations in optical properties (such as the refractive index (RI)) of graphene oxide (GO) when exposed to gases in the visible spectral region, using the thin-film interference method. The dynamic variations in the complex refractive index of GO in response to exposure to a gas is an important factor affecting the performance of GO-based gas sensors. In contrast to the conventional ellipsometry, this method alleviates the need of selecting a dispersion model from among a list of model choices, which is limiting if an applicable model is not known *a priori*. In addition, the method used is computationally simpler, and does not need to employ any functional approximations. Further advantage over ellipsometry is that no bulky optics is required, and as a result it can be easily integrated into the sensing system, thereby allowing the reliable, simple, and dynamic evaluation of the optical performance of any GO-based gas sensor. In addition, the derived values of the dynamically changing RI values of the GO layer obtained from the method we have employed are corroborated by comparing with the values obtained from ellipsometry.

References and links

1. D. Chen, H. Feng, and J. Li, "Graphene oxide: preparation, functionalization, and electrochemical applications," Chem. Rev. **112**(11), 6027–6053 (2012).
2. W. Yuan and G. Shi, "Graphene-based gas sensors," J. Mater. Chem. A Mater. Energy Sustain. **1**(35), 10078–10091 (2013).
3. A. Lipatov, A. Varezhnikov, P. Wilson, V. Sysoev, A. Kolmakov, and A. Sinitskii, "Highly selective gas sensor arrays based on thermally reduced graphene oxide," Nanoscale **5**(12), 5426–5434 (2013).
4. S. Prezioso, F. Perrozzi, L. Giancaterini, C. Cantalini, E. Treossi, V. Palermo, M. Nardone, S. Santucci, and L. Ottaviano, "Graphene oxide as a practical solution to high sensitivity gas sensing," J. Phys. Chem. C **117**(20), 10683–10690 (2013).
5. G. Ko, H.-Y. Kim, J. Ahn, Y.-M. Park, K.-Y. Lee, and J. Kim, "Graphene-based nitrogen dioxide gas sensors," Curr. Appl. Phys. **10**(4), 1002–1004 (2010).
6. H. J. Yoon, D. H. Jun, J. H. Yang, Z. Zhou, S. S. Yang, and M. M.-C. Cheng, "Carbon dioxide gas sensor using a graphene sheet," Sens. Actuators B Chem. **157**(1), 310–313 (2011).
7. M. Cittadini, M. Bersani, F. Perrozzi, L. Ottaviano, W. Wlodarski, and A. Martucci, "Graphene oxide coupled with gold nanoparticles for localized surface plasmon resonance based gas sensor," Carbon **69**, 452–459 (2014).
8. S. Tabassum, Q. Wang, W. Wang, S. Oren, M. A. Ali, R. Kumar, and L. Dong, "Plasmonic crystal gas sensor incorporating graphene oxide for detection of volatile organic compounds," in *Proceedings of IEEE 29th International Conference on Micro Electro Mechanical Systems* (IEEE, 2016), pp. 913–916.
9. S. Tabassum, R. Kumar, and L. Dong, "Plasmonic crystal based gas sensor towards an optical nose design," IEEE Sens. J. **17**(19), 6210–6223 (2017).
10. S. Tabassum, Y. Wang, J. Qu, Q. Wang, S. Oren, R. J. Weber, M. Lu, R. Kumar, and L. Dong, "Patterning of nanophotonic structures at optical fiber tip for refractive index sensing," in *Proceedings of IEEE Sensors* (IEEE, 2016), pp. 1–3.
11. S. Tabassum, R. Kumar, and L. Dong, "Nanopatterned optical fiber tip for guided mode resonance and application to gas sensing," IEEE Sens. J. **17**(22), 7262–7272 (2017).

12. M. A. Ali, S. Tabassum, Q. Wang, Y. Wang, R. Kumar, and L. Dong, "Plasmonic-electrochemical dual modality microfluidic sensor for cancer biomarker detection," in *Proceedings of IEEE 30th International Conference on Micro Electro Mechanical Systems* (IEEE, 2017), pp. 390–393.
13. M. A. Ali, S. Tabassum, Q. Wang, Y. Wang, R. Kumar, and L. Dong, "Integrated dual-modality microfluidic sensor for biomarker detection using lithographic plasmonic crystal," Lab Chip (2018), doi:10.1039/C7LC01211J.
14. M. A. Ali, C. Singh, S. Srivastava, P. Admane, V. V. Agrawal, G. Sumana, R. John, A. Panda, L. Dong, and B. D. Malhotra, "Graphene oxide-metal nanocomposites for cancer biobarker detection," RCS Adv. **7**(57), 35982–35991 (2017).
15. H. Li, J. He, S. Li, and A. P. F. Turner, "Electrochemical immunosensor with N-doped graphene-modified electrode for label-free detection of the breast cancer biomarker CA 15-3," Biosens. Bioelectron. **43**(1), 25–29 (2013).
16. S. S. Nanda, D. K. Yi, and K. Kim, "Study of antibacterial mechanism of graphene oxide using Raman spectroscopy," Sci. Rep. **6**(1), 28443 (2016).
17. S. Schöche, N. Hong, M. Khorasaninejad, A. Ambrosio, E. Orabona, P. Maddalena, and F. Capasso, "Optical properties of graphene oxide and reduced graphene oxide determined by spectroscopic ellipsometry," Appl. Surf. Sci. **421**, 778–782 (2017).
18. V. G. Kravets, O. P. Marshall, R. R. Nair, B. Thackray, A. Zhukov, J. Leng, and A. N. Grigorenko, "Engineering optical properties of a graphene oxide metamaterial assembled in microfluidic channels," Opt. Express **23**(2), 1265–1275 (2015).
19. I. Jung, M. Vaupel, M. Pelton, R. Piner, D. A. Dikin, S. Stankovich, J. An, and R. S. Ruoff, "Characterization of thermally reduced graphene oxide by imaging ellipsometry," J. Phys. Chem. C **112**(23), 8499–8506 (2008).
20. S. Cheon, K. D. Kihm, H. Kim, G. Lim, J. S. Park, and J. S. Lee, "How to reliably determine the complex refractive index (RI) of graphene by using two independent measurement constraints," Sci. Rep. **4**(1), 6364 (2015).
21. M. Turowski, T. Amotchkina, H. Ehlers, M. Jupé, and D. Ristau, "Calculation of optical and electronic properties of modeled titanium dioxide films of different densities," Appl. Opt. **53**(4), A159–A168 (2014).
22. A. J. Cohen, P. Mori-Sánchez, and W. Yang, "Insights into current limitations of density functional theory," Science **321**(5890), 792–794 (2008).
23. Z. H. Ni, H. M. Wang, J. Kasim, H. M. Fan, T. Yu, Y. H. Wu, Y. P. Feng, and Z. X. Shen, "Graphene thickness determination using reflection and contrast spectroscopy," Nano Lett. **7**(9), 2758–2763 (2007).
24. M. Bruna and S. Borini, "Optical constants of graphene layers in the visible range," Appl. Phys. Lett. **94**(3), 031901 (2009).
25. D. A. Minkov, "Calculation of the optical constants of a thin layer upon a transparent substrate from the reflection spectrum," J. Phys. D Appl. Phys. **22**(8), 1157–1161 (1989).
26. S. H. Fei, W. Can, S. Z. Pei, Z. Y. Liang, J. K. Juan, and Y. G. Zhen, "Transparent conductive reduced grahene oxide thin films produced by spray coating," Sci. China Phys. Mech. Astron. **58**(1), 014202 (2015).
27. R. Ramachandran, M. Saranya, P. Kollu, B. P. C. Raghupathy, S. K. Jeong, and A. N. Grace, "Solvothermal synthesis of Zinc sulfide decorated graphene (ZnS/G) nanocomposites for novel supercapacitor electrodes," Elect. Acta **178**, 647–657 (2015).
28. S.-H. Hong and J.-K. Song, "Comment on "Tunable Design of Structural Colors Produced by Pseudo-1D Photonic Crystals of Graphene Oxide" and Thin-Film Interference from Dried Graphene Oxide Film," Small **13**(15), 1603125 (2017).
29. K. A. Aly and F. M. A. Rahim, "Effect of Sn addition on the optical constants of Ge-Sb-S thin films based only on their measured reflectance spectra," J. Alloys Compd. **561**, 284–290 (2013).
30. C.-B. Yu, Y. Wu, X.-L. Liu, B.-C. Yao, F. Fu, Y. Gong, Y.-J. Rao, and Y.-F. Chen, "Graphene oxide deposited microfiber knot resonator for gas sensing," Opt. Mater. Express **6**(3), 727–733 (2016).
31. B. Mehta, K. D. Benkstein, S. Semancik, and M. E. Zaghloul, "Gas sensing with bare and graphene-covered optical nano-antenna structures," Sci. Rep. **6**(1), 21287 (2016).
32. S. Al-Zangana, M. Iliut, G. Boran, M. Turner, A. Vijayaraghavan, and I. Dierking, "Dielectric spectroscopy of isotropic liquids and liquid crystal phases with dispersed graphene oxide," Sci. Rep. **6**(1), 31885 (2016).
33. J. A. Woollam Co, Inc, "A short course in ellipsometry," https://www.nnf.ncsu.edu/sites/default/files/vase_manual_short_course.pdf.
34. D. Poelman and P. F. Smet, "Methods for the determination of the optical constants of thin films from single transmission measurements: a critical review," J. Phys. D Appl. Phys. **36**(15), 1850–1857 (2003).

1. Introduction

Graphene has attracted recent attention as a versatile sensing material, due to its sensitive electronic and optical properties, and ability to bind with many analytes. Because of large surface area-to-volume ratio [1] and remarkably high carrier mobility of graphene at room temperature (200,000 cm^2 V^{-1} s^{-1}) [2], graphene-based materials have been explored extensively in sensing, e.g., for gas [3–11] and biological applications [12–15]. The enormous potential of graphene-based materials in detecting minute concentrations of chemical and

biological analytes due to the changes in its optical properties caused by the adsorption of the gases or analytes has led to a rising interest in utilizing graphene and its derivatives as gas adsorption and sensing materials. When the gas-sensing performance of pristine graphene is low owing to weaker adsorption of gas molecules on its surface, further functionalization of graphene is performed to improve its sensing performance. One such derivative of graphene is graphene oxide (GO), which is a two-dimensional monolayer comprising different oxygen containing functionalities (e.g., carboxyl, hydroxyl, carbonyl, and epoxide) with a very high sensitivity to surface adsorbates [16], hence making GO a promising choice for highly sensitive sensing material.

The knowledge of the changes in the optical parameters, namely, the complex refractive indices, of a material in response to adsorbed gases is necessary in designing a sensor based on the light transmission or reflection measurements. So, for example the optical properties of GO in a GO-based optical gas sensor are an important factor affecting its sensing performance, which vary depending on the amount of adsorbed gas species in the GO layer. Accordingly, and owing to a growing interest in studying GO as a sensing material, evolution of RI values of GO nanosheets upon their exposure to the ambient environment are worthy of investigation. In our recent works, we have developed plasmonic crystal [8,9] and guided mode resonance-based nanostructures [10, 11], integrated with GO, to work as gas sensors, wherein the dynamic response of the sensor has been studied when exposed to gases. In such applications, studying the optical properties of GO is inevitably required to predict the sensor performance. A knowledge of the refractive index (RI) values facilitates the verification of the experimental results against a theoretical model.

The refractive index of a material is in general a complex number, corresponding to the change in propagation speed of light through it owing to the dielectric interactions plus the losses caused by the ionic interactions, and varies with the wavelength. Several research efforts have been reported which studied the complex refractive index, and among those, ellipsometry is a popular reliable method to characterize the optical properties of the GO nanosheets [17–19]. Ellipsometry exploits the changes in the polarization state of the light reflected from a thin film of the material being probed to infer the optical properties (see the details provided in the Appendix). However, this requires choosing a fitting model (from among a number of model choices) to deduce the complex RI of the material from the measured intensity of p- and s- polarizations at different phase alignments. Choosing a correct fitting model requires a priori expert knowledge about the material, which may not always be available and becomes a limitation for ellipsometry. Further the models themselves are highly complex, involving multiple equations, leading to higher chances of numerical issues (such as getting trapped in a local optimum).

There exist other methods to compute the RI of a thin film such as the ATR (attenuated total reflection) intensity, DFT (density function theory), and RS (reflection spectroscopy) measurements. Cheon et al. determined the complex RI of graphene using two independent measurements, namely (i) measuring the light absorption by a thin gold (Au) layer coated with graphene at the SPR (surface plasmon resonance) critical angle, and (ii) using the ATR to measure the reflectance ratio of p-polarized to s-polarized light (R_p/R_s) wherein the incident light is attenuated by a bare graphene layer [20]. Thus a reliable determination of complex RI of graphene was possible using two independent methods, and without using any target model fitting elaboration as in the case of ellipsometry. However, the SPR and ATR measurements are based on prism-coupling which makes the optical setup bulky and expensive. The DFT approach for finding the optical properties of a material is based on simulating the interactions between electrons in the material [21]. This method is widely applied for practical reasons that its simple approximations work well in predicting the structure of a material. But, DFT based RI calculations suffer from large errors because of the approximations made in constructing the exchange-correlation functionals [22]. In another report, Ni et al. [23] employed RS to compute the thickness of graphene. But, their

computation was based on an overly simplified assumption of constant RI values of graphene in the entire visible range, which is unrealistic. Later, Bruna et al. modeled only the imaginary part of complex RI of graphene while keeping the real part constant [24]. So, there exists a need for developing an alternative that is experimentally and computationally simple to determine the complex RI of GO, overcoming the aforementioned limitations.

In contrast to the above methods, the thin-film interference that we employ utilizes only the maximum and minimum of the reflectance spectrum in order to compute the RI. The method is computationally simple, and does not need to employ any functional approximations, resulting in highly accurate and reliable results. Also, to the best of our knowledge, our work provides a first systematic experimental study to characterize the *dynamically evolving* optical properties of GO nanosheets in response to exposure to gas species. (As time progresses, more gases are adsorbed, causing higher changes in the RI values.)

In this paper, we characterize the dynamic evolution of the RI values of a GO thin film in response to exposure to a gas (namely, ammonia) by the method of thin-film interference as developed by Minkov [25]. We measured reflectance spectra of a GO thin film coated on a glass substrate over the visible spectra and at room temperature. The interaction of a probe beam reflected from multiple interfaces (air-film and film-glass) results in interference fringes in the reflection spectra. These reflection spectra of a GO thin film were monitored in response to exposure to ammonia, and analyzed to determine the dynamically evolving complex RI of the GO thin film. This sensitivity of RI to exposed gas concentration is crucial to the performance of the GO-based optical sensors. Finally, we compare our findings with results obtained by ellipsometry. Note, while ellipsometry is accurate, and hence we use it for comparison, it is not practical to be employable in studying the dynamic changes in RI of GO in response to exposure to analyte. Apart from the complexity of fitting model selection, physical constraints arise with using ellopsometry: gas sensing requires an enclosed experimental setup for which it is often not possible to integrate with a commercially available ellipsometer. In contrast, using the thin-film interference method that we use is (i) computationally universal (requiring no fitting model selection) and simpler (deals with an order less number of equations), (ii) highly accurate being based on only the reflectance spectra peaks, and also (iii) physically integrable into sensing system (so dynamically changing RI can be measured while sensing is occurring). The key contributions of our work are as follows:

- Experimentally compute the *dynamic changes* in the refractive index (RI) of GO in a relatively simple and straightforward yet effective manner utilizing the theoretical foundation laid in [25].

- Demonstrate through experimental setup that the approach is physically integrable into the sensing system, which is a required attribute for being able to observe the dynamically changing RI in response to ongoing interaction with the analyte.

2. Details of the experimentation methods

2.1 GO thin film preparation method

To prepare a GO thin film on a glass substrate, aqueous suspensions of GO nanosheets (1 mg/mL) were prepared by thoroughly dispersing 1 mg of the synthesized GO nanosheet flakes (purchased from Graphene Supermarket) in 1 mL of deionized water, followed by sonication at room temperature for 90 min [8]. The GO dispersion solution was then sprayed onto a microscope glass slide using an airbrush (Badger 350, Badger Air-Brush Co.) [26]. The substrate was next dried at room temperature for 6 hrs, which let the remaining GO sheets to form a uniform thin film on the glass slide.

2.2 Characterization and measurement methods

The complex refractive index as well as the average thickness of GO thin film coated on glass substrate were determined from the thin-film interference fringes in the reflection spectra, following the method developed by Minkov [25]. A bifurcated optical fiber (BIF 400-VIS-NIR, Ocean Optics)—see Fig. 1(a)—was used to illuminate the sensor from a white light source (150 watt quartz halogen lamp, Luxtec Fiber Optics) through a collimator (F220SMA-A, Thorlabs), and to collect the reflected light from the GO surface into a spectrometer (USB-4000, Ocean Optics). We measured the reflectance spectra for a normal incident light. The optical setup and the measured reflection spectrum of the GO thin film are depicted in Figs. 1(a) and 1(b) respectively.

The scanning electron microscopy (SEM) analysis was performed to characterize the GO film coated on glass. The top-view and cross-section of GO thin film on glass substrate are shown in Fig. 1(c). From the cross-section view, the thickness of the GO film was found to be approximately 650 nm.

Raman spectroscopy was also conducted to further characterize the GO film on glass. The Raman spectrum of GO depicts the characteristic peaks of D and G at 1354 cm^{-1} and 1598 cm^{-1} respectively (Fig. 1(d)). The D band corresponds to the presence of disorders in the GO nanosheets, whereas the G band is associated with C-C bond stretch in sp2 carbon domains [27].
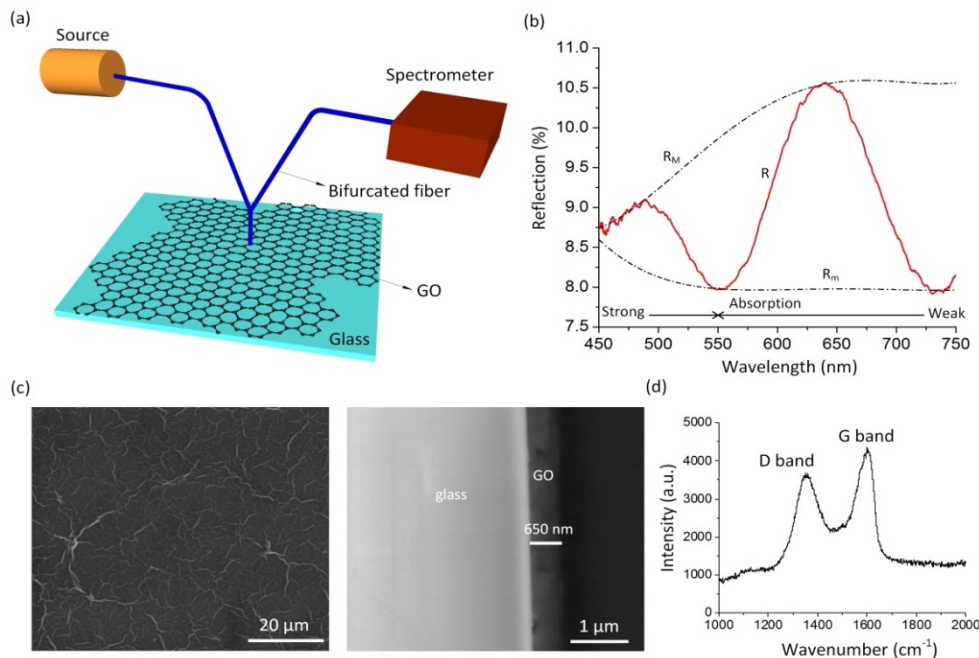

Fig. 1. (a) Schematic illustration of optical setup for characterizing the optical properties of a GO thin film. (b) Reflection spectrum R of the GO thin film in air and the envelopes R_m and R_m as fitted to the maxima and minima of R, respectively. (c) SEM images of GO thin film on glass: top view (left) and cross section (right). (d) Raman spectrum of GO.

3. Determining the refractive index from interference fringes

We first provide the underlying principle. Suppose the GO thin film has a thickness t and a complex refractive index $\eta = \eta + ik$, where η is the refractive index and k the extinction coefficient and can be related to the absorption coefficient $\alpha = 4\pi k / \lambda$, where λ is the

wavelength of light. The glass substrate has a thickness several orders of magnitude larger than t and has index of refraction, denoted η_s. The interference fringes observed in the reflection spectrum of the GO film, are shown in Fig. 1(b). Such fringes in the reflectance spectrum of GO have also been observed in [28]. The interference fringes occur due to the reflections from the two interfaces, namely, air-GO and GO-glass interfaces. These fringes

can be used to calculate the RI values of GO, noting that the reflectance R is a function of $\eta, k, \eta_s, t, \lambda$ [25]:

$$R = \frac{A' - (B_1' \cos 2\delta - B_2' \sin 2\delta)x + C'x^2}{A^* - (B_1^* \cos 2\delta - B_2^* \sin 2\delta)x + C^*x^2} + \frac{A''x^2}{A^* - (B_1^* \cos 2\delta - B_2^* \sin 2\delta)x + C^*x^2} *$$

$$\frac{1}{D'' - (E_1^* \cos 2\delta - E_2^* \sin 2\delta)x + F^*x^2} \tag{1}$$

where,

$$A' = [(\eta-1)^2 + k^2][(\eta+\eta_s)^2 + k^2]$$

$$B_1' = 2\left[(\eta^2 + k^2 - 1)(\eta^2 + k^2 - \eta_s^2) + 4k^2\eta_s\right]$$

$$B_2' = 4k[\eta_s(\eta^2 + k^2 - 1) - (\eta^2 + k^2 - \eta_s^2)]$$

$$C' = [(\eta+1)^2 + k^2][(\eta-\eta_s)^2 + k^2]$$

$$A^* = [(\eta+1)^2 + k^2][(\eta+\eta_s)^2 + k^2]$$

$$B_1^* = 2\left[(\eta^2 + k^2 - 1)(\eta^2 + k^2 - \eta_s^2) - 4k^2\eta_s\right]$$

$$B_2^* = 4k\left[\eta_s(\eta^2 + k^2 - 1) + (\eta^2 + k^2 - \eta_s^2)\right]$$

$$C^* = [(\eta-1)^2 + k^2][(\eta-\eta_s)^2 + k^2]$$

$$A'' = 64\eta_s(\eta_s - 1)^2(\eta^2 + k^2)^2$$

$$D'' = [(\eta+1)^2 + k^2][(\eta+1)(\eta+\eta_s^2) + k^2]$$

$$E_1^* = 2\left[(\eta^2 + k^2 - 1)(\eta^2 + k^2 - \eta_s^2) - 2k^2(\eta_s^2 + 1)\right]$$

$$E_2^* = 2k\left[(\eta^2 + k^2 - \eta_s^2) + (\eta_s^2 + 1)(\eta^2 + k^2 - 1)\right]$$

$$F^* = [(\eta-1)^2 + k^2][(\eta-1)(\eta-\eta_s^2) + k^2]$$

$x = \exp(-\alpha t)$ and $\delta = \dfrac{2\pi\eta t}{\lambda}$

Noting that α is a function of k, λ, the above parameters are functions of $\eta, k, \eta_s, t, \lambda$ the first 4 of which are unknowns and need to be determined, while the parameter λ is measured.

The extremes of the interference fringes, represented by the envelopes R_M and R_m (see Fig. 1(b)) are given as [25]:

$$R_M = \frac{(ad + bcx)^2}{(bd + acx)^2} + \frac{gx^2}{(bd + acx)^2(b^3f + 2abcdx + a^3ex^2)}$$

$$R_m = \frac{(ad - bcx)^2}{(bd - acx)^2} + \frac{gx^2}{(bd - acx)^2(b^3f - 2abcdx + a^3ex^2)} \tag{2}$$

where, $a = \eta - 1$, $b = \eta + 1$, $c = \eta - \eta_s$, $d = \eta + \eta_s$, $e = \eta - \eta_s^2$, $f = \eta + \eta_s^2$ and $g = 64\eta_s (\eta_s - 1)^2 \eta^4$. Note all these parameters are functions of η and η_s, and since x is a function of k, t, λ, ultimately, R_M, R_m are functions of η, k, η_s, t. So by measuring R_M, R_m as functions of λ, we can determine the unknowns η, k, η_s, t. In particular, in the transparent region of the spectrum, the refractive index of glass substrate, η_s can be determined as [25]:

$$\eta_s = \frac{1 + [R_m(2 - R_m)]^{1/2}}{1 - R_m} \tag{3}$$

Further, a basic equation for interference fringes that can be used to determine the thickness t is [25]:

$$4\eta t = m\lambda \tag{4}$$

where, an odd order number m corresponds to the wavelength for which R has a maximum, and even order number m corresponds to wavelength for which R has a minimum (see Fig. 1(b) for R versus R_m versus R_M). It follows from Eq. (4) that if η_1 and η_2 are the refractive indices calculated from a pair of adjacent extrema that correspond to the wavelengths λ_1 and λ_2, respectively, then the film thickness can be determined using [25]:

$$t = \frac{\lambda_1 \lambda_2}{4(\lambda_1 \eta_2 - \lambda_2 \eta_1)} \tag{5}$$

In summary, the steps to determine the complex refractive index of GO that we used are as listed below:

1. To start, the refractive index of the glass substrate η_s was calculated from the envelope R_m in the spectral region of weak absorption, using Eq. (3). For example, in Fig. 1(b), in the weak absorption region $R_m = 8\%$, providing $\eta_s = 1.51$, which is a typical average value of RI for glass in the visible spectral region. The reflectance (and hence refractive index) of bare glass was almost constant in the visible spectral region (using Eq. (3)). This is also supported by the observations in [29]. Further, we also measured the optical constants of the same sample using ellipsometry, and the results were found close to the values calculated using thin-film interference. The ellipsometry results are demonstrated later in Fig. 3. The proximity of the measurements from the two approaches (ellipsometry vs. thin-film interference) confirms that the refractive index change of glass, if any, was not significant to influence the results of RI measurements of the thin-film GO.

2. Next, Newton-Raphson iteration was used to solve the system of two equations Eq. (2) for the two unknowns η and x (where note that η_s is known at this point from the first step above), using the measured values of R_M and R_m which are the peaks and valleys of the interference spectrum respectively (values listed in Table 1). In order to achieve faster convergence, computations were started for λ in the weak absorption region ($\lambda = 734.6$ nm), where the initial estimate x^0 was presumed to be 0.8, and similarly an initial estimate was chosen for η^0 [25]. For the $(j+1)$ th iteration, η^j and x^j values were used from the previous j th iteration, and the final converged values of refractive index and absorbance were denoted η and x respectively.

3. In order to calculate η and x values for a next λ value, η and x values obtained for the previous extremum were used as initial estimates. For example, to obtain η and x values of GO film in air and at λ = 640.2 nm, η^0 = 1.86 and x^0 = 0.2289 obtained for λ = 734.6 nm were used as initial estimates. The same procedure was followed for all the successive λ values. Thus, the η and x columns listed in Table 1 were obtained.

4. The next step was to estimate the GO thickness, t using the η values of two neighboring extrema by applying Eq. (5). Accordingly, various estimates of thickness t of the GO film as listed in Table 1 were obtained, and from which the averaged value $\bar{t}$ was calculated.

5. Subsequently, the order numbers m were calculated by substituting η and the average value $\bar{t}$ of thicknesses for all the wavelengths, in Eq. (4). The order numbers m were next approximated as the consecutive integers.

6. Next, the accuracy of t was significantly increased by taking the m values associated to each extremum and deriving a new thickness approximation t^f, where t^f was calculated by substituting the values of η and m in Eq. (4). This was also confirmed by noting that the values of t^f have smaller variances compared to t values ($\sigma_{t^f} \ll \sigma_t$).

7. The final value of refractive index η^f was found from Eq. (4) using the calculated values of the average thickness, $\overline{t^f}$ and order numbers, m.

8. Finally, the value of extinction coefficient, k for each λ was found by solving Eq. (1) for the envelope R_M, using again the Newton-Raphson iteration.

4. Experimental description, results, and discussion

The RI values of GO were determined in air and in presence of ammonia (NH_3) gas, using the method described in the section above. Gaseous ammonia (pre-diluted with the carrier gas of dry nitrogen) flowed from a cylinder into an aluminum gas chamber which contained the GO coated glass slide. The gas flow rate was controlled by a mass flow controller (MFC) (GFC17, Aalborg). Inside the chamber, the testing gas was further diluted by the carrier nitrogen gas. A constant flow rate of dry nitrogen (10 ml/min) was maintained inside the closed chamber and flow rate of ammonia was varied at regular intervals using the MFCs to modify the concentration of the gaseous ammonia. The GO thin film was illuminated from a white light source through a bifurcated fiber and the reflected light was collected by a spectrometer. From the flow rates of ammonia and nitrogen gases, the ppm level of gaseous ammonia was obtained by doing some mathematical calculations. Also, prior to the dynamic measurements of gaseous ammonia mixed with nitrogen, the baseline response was monitored in presence of only the nitrogen gas.

   No observable change in interference pattern was observed for ammonia concentrations below 200 ppm, while the response saturated at 500 ppm. Also, while the measurements were taken at four different wavelengths of 734.6 nm, 640.2 nm, 551.5 nm, and 489.9 nm, it turned out that at 489.9 nm, the optical absorption was dominant, dampening the interference fringes. Consequently, the results were not reliable, and we chose to omit the extinction coefficient data at 489.9 nm. Subsequent to the measurements, we purged the GO thin film with dry nitrogen and next with heating at 70°C for approximately 2 hrs to completely desorb the gas molecules from the film. This is required to perform a next experiment. The heating

process restored the initial refractive index of the bare GO film as confirmed by the baseline measurements.

Figures 2(a) and 2(b) demonstrate the shift in intereference patterns of the GO with exposure to ammonia gas over a 44 min period, resulting in a dynamically evolving RI. The presence of a strong interference oscillations above 550 nm implies a spectral region of weak absorption. The onset of stronger absorption below 550 nm is represented as dampening of the fringes. The calculated values of η and k from the envelopes R_M and R_m of the reflectance spectrum of a GO thin film, shown in Fig. 2(a), are tabulated in Table 1. Note while the final thickness and final refractive index after iteration are more accurate, the intermediate values of refractive index and thickness are shown to illustrate all the steps of the algorithm. It shows the progress of the iterative computations, showing the completeness of the work. Only the final thickness and final refractive index were used to draw conclusions and make comparison with ellipsometry.

4.1 Dynamic variations in η^f and k and thickness calculation

The dynamic variations of η^f and k values of the GO nanosheets exposed to three different concentrations of ammonia gas (200 ppm, 300 ppm, and 500 ppm), are illustrated in Figs. 2(c) and 2(d). Additionally, Table 1 also summarizes the dynamic variation in RI of GO by listing in successive columns, the values of R_M, R_m, η, x, t, m, t^f, η^f, k, while the rows list the wavelengths at which the column values are computed. The rows are further organized in successive blocks corresponding to the values after each additional 4 mins of gas exposure (so with a total of 44 mins of gas exposure, there are a total of 12 blocks, where the 1st block is for time zero).

The calculated values of η^f and k of the GO film in air are 1.8714 and 0.1613 respectively at the wavelength of 640.2 nm. Initally, the sensor was exposed to 200 ppm of gaseous ammonia. It can be observed that the η^f values of GO increased over time as it was exposed to the gas for longer and longer times. This is expected because the large number of functional groups at the GO surface can effectively capture the gas molecules which enhances the RI of GO [30, 31]. In the beginning, for each wavelength, the rate of increase of η^f was high. However, after 8 min, the rate of increase slowed down and at approximately 16 min, η^f values started to saturate, likely because the gas molecules already remaining in the GO layer inhibited further interaction and hence adsorption of newer gas molecules. After the sensor response was saturated to $\eta^f = 1.883$ for 200 ppm of ammonia gas (for $\lambda = 640.2$ nm), the sensor was successively exposed to 300 ppm, and 500 ppm of gaseous ammonia. The η^f values of the GO thin film increased successively by 0.0116, 0.0009, and 0.0011 refractive index unit (RIU) in response to 200 ppm, 300 ppm, and 500 ppm ammonia gas respectively. Similarly, extinction coefficient curve, k which accounts for light absorption by the GO film initially increased over time and saturated after some time for each concentration of gaseous ammonia. The calculated average thickness of GO thin film in air was 624 nm (Table 1) which is close to 650 nm, the actual thickness observed from SEM analysis (Fig. 1(c)). In the plot of η and k vs. the wavelength (Fig. 3), the peak at 640 nm suggests the occurrence of a dielectric relaxation mode of the GO layer. Similar phenomena has also been observed in [32].
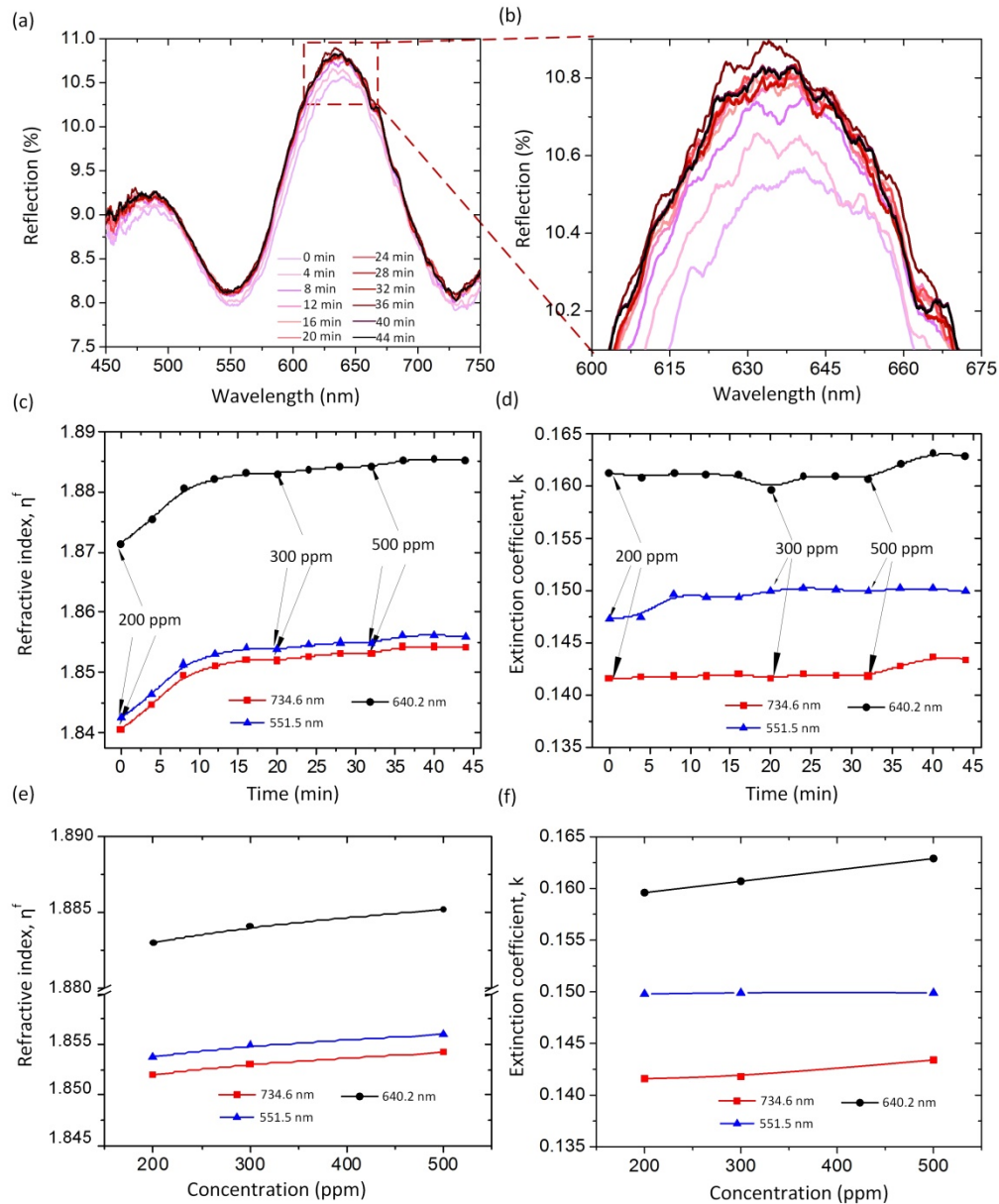
Fig. 2. (a) Dynamic evolution of reflectance spectra upon exposure to ammonia gas over 44 mins. (b) Zoomed-in spectra from the region denoted by red dashes in (a), emphasizing the shifts in interference fringes in response to gas exposure. Dynamic variation of (c) refractive index and (d) extinction coefficient in exposure to ammonia gas and at different wavelengths of light. Arrows denote the instants at which the GO thin film was exposed to 200, 300 and 500 ppm of ammonia gas. Shifts in (e) refractive index and (f) extinction coefficient as a function of concentration of ammonia gas.

4.2 Sensitivity studies

Figures 2(e) and 2(f) show shifts in RI values with a change in gas concentration. The η^f and k sensitivity of the sensor in response to ammonia gas was found to be 6.5×10^{-6} RIU/ppm and 9.86×10^{-6} RIU/ppm respectively at $\lambda = 640.2$ nm. The lower sensitivities at wavelengths

of 734 nm and 551 nm suggest that λ = 640.2 nm is better suited for optical sensing. Here, refractive index (RI) is defined in the standard way as the ratio of speed of light in vacuum to the speed of light in the medium. The sensitivity in terms of RIU/ppm provides the change in refractive index of the GO film against the change in gas concentration.

5. Comparison to ellipsometry

The experimentally determined RI values of bare GO film (without the presence of any gas) in this work were further compared to the RI values of the same sample measured using ellipsometry. This is shown in the Fig. 3 below. The measured results using ellipsometry were found close to the values calculated using thin-film interference, with a maximum variation of ~0.4%, adding confidence to our method and results. This verifies the accuracy of thin-film interference method in computing RI of GO. The error bars represent a maximum standard deviation of ~ ± 0.2%. The dynamic measurement of RI values of GO in response to exposure to gas is a unique and novel feature to our study, absent in prior studies [17–19].

Table 1. The calculated values of complex refractive index ($\eta + ik$) and thickness (t) of GO are based on the fringe interference method [25]

λ (nm)	R_M (%)	R_m (%)	η	x	t (nm)	m	t^f (nm)	η^f	k
					in air				
734.6	10.55	7.960	1.8600	0.2289	667	6	592	1.8405	0.1416
640.2	10.55	7.977	1.8609	0.2268	573	7	602	1.8714	0.1613
551.5	9.878	7.977	1.8436	0.1770	633	8	598	1.8424	0.1473
489.9	9.112	8.189	1.8311	0.0895	-	9	602	1.8412	-

$\overline{t}$ = 624 nm, σ_t = 47 nm, $\overline{t^f}$ = 598 nm, σ_{t^f} = 4.5 nm

λ (nm)	R_M (%)	R_m (%)	η	x	t (nm)	m	t^f (nm)	η^f	k
				After 4min of exposure to ammonia gas					
734.6	10.63	8.029	1.8654	0.2259	668	6	590	1.8446	0.1417
640.2	10.63	8.027	1.8653	0.2262	572	7	600	1.8755	0.1608
551.5	9.950	8.027	1.8478	0.1765	638	8	597	1.8464	0.1475
489.9	9.150	8.218	1.8334	0.0895	-	9	601	1.8452	-

$\overline{t}$ = 626 nm, σ_t = 49 nm, $\overline{t^f}$ = 597 nm, σ_{t^f} = 4.8 nm

λ (nm)	R_M (%)	R_m (%)	η	x	t (nm)	m	t^f (nm)	η^f	k
				After 8min of exposure to ammonia gas					
734.6	10.73	8.091	1.8710	0.2253	667	6	589	1.8496	0.1418
640.2	10.72	8.084	1.8704	0.2254	572	7	599	1.8806	0.1612
551.5	10.02	8.084	1.8522	0.1752	634	8	595	1.8514	0.1497
489.9	9.220	8.292	1.8384	0.0878	-	9	599	1.8502	-

$\overline{t}$ = 624 nm, σ_t = 48 nm, $\overline{t^f}$ = 595 nm, σ_{t^f} = 4.8 nm

λ (nm)	R_M (%)	R_m (%)	η	x	t (nm)	m	t^f (nm)	η^f	k
				After 12min of exposure to ammonia gas					
734.6	10.76	8.109	1.8726	0.2251	666	6	588	1.8511	0.1418
640.2	10.75	8.102	1.8720	0.2253	571	7	598	1.8821	0.1611
551.5	10.05	8.102	1.8538	0.1753	634	8	595	1.8530	0.1494
489.9	9.250	8.305	1.8398	0.0890	-	9	599	1.8518	-

$\overline{t}$ = 624 nm, σ_t = 48 nm, $\overline{t^f}$ = 595 nm, σ_{t^f} = 4.8 nm

λ (nm)	R_M (%)	R_m (%)	η	x	t (nm)	m	t^f (nm)	η^f	k
				After 16min of exposure to ammonia gas					
734.6	10.78	8.119	1.8736	0.2253	666	6	588	1.8522	0.1420
640.2	10.77	8.112	1.8730	0.2255	571	7	598	1.8832	0.1611
551.5	10.07	8.112	1.8548	0.1757	633	8	594	1.8541	0.1493
489.9	9.271	8.321	1.8411	0.0891	-	9	598	1.8528	-

$\overline{t}$ = 623 nm, σ_t = 48 nm, $\overline{t^f}$ = 595 nm, σ_{t^f} = 4.8 nm

λ (nm)	R_M (%)	R_m (%)	η	x	t (nm)	m	t^f (nm)	η^f	k
				After 20min of exposure to ammonia gas					
734.6	10.78	8.114	1.8734	0.2259	666	6	588	1.8520	0.1416
640.2	10.78	8.105	1.8729	0.2270	572	7	598	1.8830	0.1596
551.5	10.06	8.105	1.8542	0.1757	631	8	594	1.8538	0.1498

| 489.9 | 9.254 | 8.334 | 1.8411 | 0.0862 | - | 9 | 598 | 1.8526 | - |

$$\overline{t} = 623 \text{ nm}, \; \sigma_t = 47 \text{ nm}, \; \overline{t^f} = 595 \text{ nm}, \; \sigma_{t^f} = 4.8 \text{ nm}$$

After 24min of exposure to ammonia gas									
734.6	10.79	8.127	1.8742	0.2250	665	6	588	1.8527	0.1420
640.2	10.78	8.123	1.8738	0.2248	572	7	598	1.8837	0.1610
551.5	10.07	8.123	1.8553	0.1744	634	8	594	1.8545	0.1503
489.9	9.265	8.328	1.8412	0.0878	-	9	598	1.8533	-

$$\overline{t} = 624 \text{ nm}, \; \sigma_t = 47 \text{ nm}, \; \overline{t^f} = 594 \text{ nm}, \; \sigma_{t^f} = 4.8 \text{ nm}$$

After 28min of exposure to ammonia gas									
734.6	10.80	8.135	1.8749	0.2247	666	6	587	1.8532	0.1419
640.2	10.79	8.127	1.8742	0.2250	571	7	597	1.8842	0.1609
551.5	10.08	8.127	1.8558	0.1747	634	8	594	1.8550	0.1501
489.9	9.270	8.332	1.8415	0.0878	-	9	598	1.8538	-

$$\overline{t} = 624 \text{ nm}, \; \sigma_t = 48 \text{ nm}, \; \overline{t^f} = 594 \text{ nm}, \; \sigma_{t^f} = 4.9 \text{ nm}$$

After 32min of exposure to ammonia gas									
734.6	10.80	8.134	1.8748	0.2249	666	6	587	1.8531	0.1418
640.2	10.79	8.126	1.8742	0.2251	571	7	597	1.8841	0.1607
551.5	10.08	8.126	1.8557	0.1748	635	8	594	1.8549	0.1499
489.9	9.267	8.330	1.8413	0.0878	-	9	598	1.8537	-

$$\overline{t} = 624 \text{ nm}, \; \sigma_t = 48 \text{ nm}, \; \overline{t^f} = 594 \text{ nm}, \; \sigma_{t^f} = 4.9 \text{ nm}$$

After 36min of exposure to ammonia gas									
734.6	10.81	8.139	1.8753	0.2249	665	6	587	1.8543	0.1428
640.2	10.80	8.132	1.8747	0.2251	570	7	597	1.8853	0.1621
551.5	10.10	8.132	1.8565	0.1756	627	8	594	1.8561	0.1502
489.9	9.319	8.369	1.8444	0.0881	-	9	597	1.8549	-

$$\overline{t} = 621 \text{ nm}, \; \sigma_t = 47 \text{ nm}, \; \overline{t^f} = 594 \text{ nm}, \; \sigma_{t^f} = 4.7 \text{ nm}$$

After 40min of exposure to ammonia gas									
734.6	10.80	8.145	1.8754	0.2236	666	6	587	1.8543	0.1436
640.2	10.79	8.134	1.8746	0.2242	570	7	597	1.8854	0.1632
551.5	10.10	8.134	1.8566	0.1754	627	8	594	1.8562	0.1502
489.9	9.324	8.365	1.8444	0.0889	-	9	597	1.8550	-

$$\overline{t} = 621 \text{ nm}, \; \sigma_t = 48 \text{ nm}, \; \overline{t^f} = 594 \text{ nm}, \; \sigma_{t^f} = 4.7 \text{ nm}$$

After 44min of exposure to ammonia gas									
734.6	10.80	8.143	1.8753	0.2238	666	6	587	1.8542	0.1434
640.2	10.79	8.132	1.8745	0.2244	570	7	597	1.8852	0.1629
551.5	10.10	8.132	1.8565	0.1756	627	8	594	1.8560	0.1499
489.9	9.322	8.363	1.8442	0.0889	-	9	597	1.8548	-

$$\overline{t} = 621 \text{ nm}, \; \sigma_t = 48 \text{ nm}, \; \overline{t^f} = 594 \text{ nm}, \; \sigma_{t^f} = 4.7 \text{ nm}$$

In contrast to ellipsometry, our method of determining the RI of GO is (i) easier, requiring no model selection, and (ii) also less time consuming. Our method employs the same algorithm to determine the complex RI of GO at different time of exposure to gas. In contrast, in ellipsometry, for each time exposure, a regression analysis needs to be performed in which model parameters are varied until the calculated and the experimental data closely match. This makes the ellipsometry much tedious and time consuming, especially for dynamic RI measurements. On the other hand, thin-film intereference method is affected with small film thickness or with highly absorbing material since those affect the formation of the interference fringes suitable for measurements.
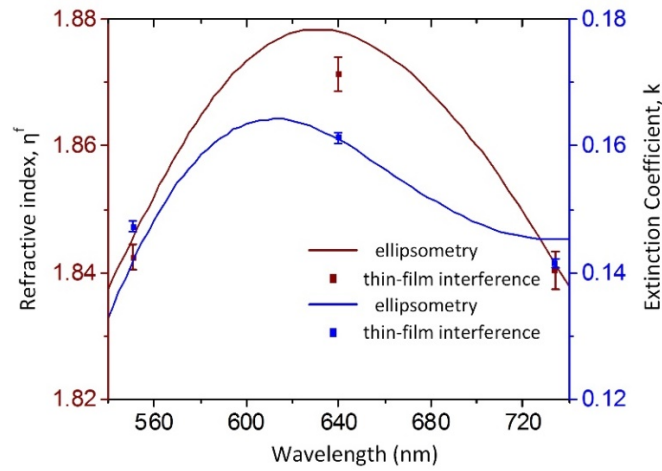
Fig. 3. Comparison of the derived complex RI of bare GO film using thin-film interference with that of ellipsometry.

6. Conclusion

We presented an effective yet simple method based on thin-film interference to determine the dynamic changes in the optical RI values of a GO thin flim in response to its exposure to the ammonia gas over time, and at multiple wavelengths. Note since the prior works only measured the RI values in air, the dynamic measurements of RI values upon exposure to gas is a unique and novel feature of our work. Also, our method, unlike ellipsometry, allows a straightforward determination of both the real and imaginary components of refractive index of GO with no need for any model fitting elaboration, is computationally simple needing an order fewer equations to solve and thus less time consuming, and is also physically integrable into the sensing system for making the dynamic RI change measurements feasible. For validating our method, we showed that the obtained RI values of the GO layer are comparable to those obtained from ellipsometry. Our method also correctly measured the film thickness, further validating its accuracy. Developing a detailed understanding of the optical properties of graphene oxide plays a significant role in characterizing the performance as an optical sensor. Thereby, the presented method of determining the optical RI values of a GO layer helps support the principle of optical sensing for GO-based gas sensors. It also provides a way to select a wavelength where the sensivity of the RI to gas concentration is the highest.

Appendix: Ellipsometry for the refractive index

Ellipsometry measures the relative change in polarization state of light reflected from a sample surface. The measured values are expressed as ψ and Δ, which, respectively, contain the information about relative amplitude ratio and phase difference of p- and s- polarized light (incident versus reflected). These two parameters are defined as:

$$tan(\psi)e^{j\Delta} = \frac{R_p}{R_s},\qquad(6)$$

where R_p and R_s are Fresnel reflection (complex) coefficients for p- and s- polarizations respectively. Thus, by measuring the reflected beam intensities, Fresnel equations along with Eq. (6) can be applied to find ψ and Δ [33].

Next, a model is constructed to infer the RI values and thickness of the material from the measured values of ψ and Δ. The known parameters of the model are wavelength, polarization state and angle of the incident light, whereas the unknown parameters are optical

RI values and thickness of the film. A wide class of dispersion equations are available to model the optical RI values of different materials: The Cauchy equations are well-suited to model transparent materials like SiO_2, Al_2O_3 Si_3N_4 etc.; the Sellmeier relation is applicable to transparent materials and semiconductors in the infrared, e.g., Si, Ge, GaAs; the Lorentz oscillator model is suitable for absorbing materials; the Forouhi-Bloomer dispersion equations are used to model crystalline semiconductors and dielectrics; the Drude model was developed to model metals; and so on [34]. In other words, there is no single model which can model all kinds of materials, thus making it necessary to have a prior knowledge of the RI dispersion of the material. Further, a regression analysis is performed wherein the unknown RI values in the constructed model are varied until the ellipsometric data (ψ and Δ) calculated from the model matches the experimental data as closely as possible. This also makes the process laborious and time consuming.